CEBAF PR-93-008
April 26, 1993

ANALYSIS OF SPACE CHARGE CALCULATION IN PARMELA AND ITS APPLICATION TO THE CEBAF FEL INJECTOR DESIGN

H. Liu
Continuous Electron Beam Accelerator Facility
12000 Jefferson Avenue
Newport News, VA 23606

CONTINUOUS
ELECTRON
BEAM
ACCELERATOR
FACILITY

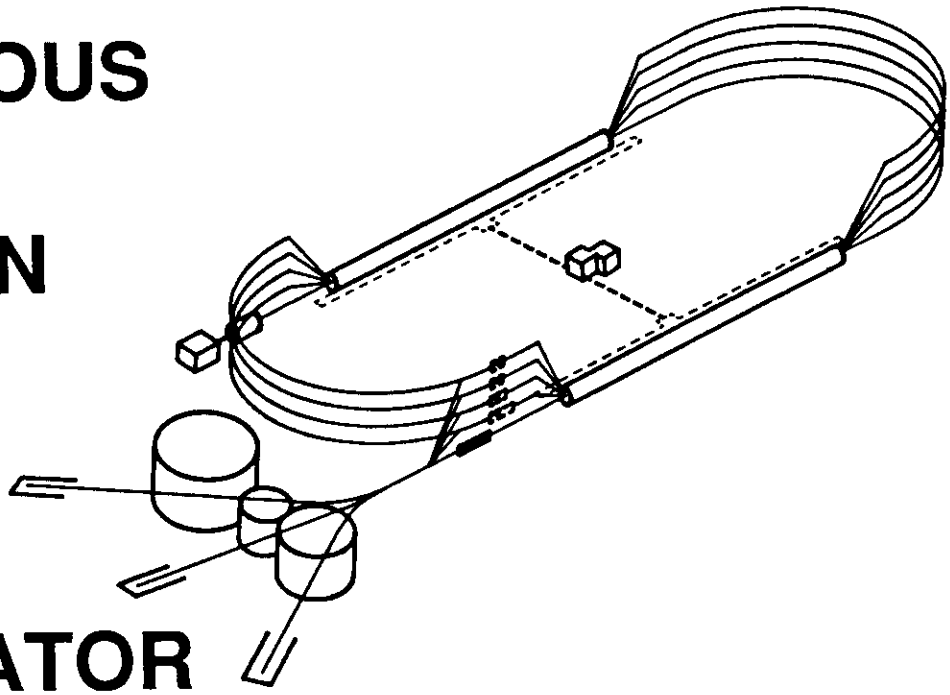

SURA Southeastern Universities Research Association

CEBAF
The Continuous Electron Beam Accelerator Facility
Newport News, Virginia

Copies available from:

Library
CEBAF
12000 Jefferson Avenue
Newport News
Virginia 23606

The Southeastern Universities Research Association (SURA) operates the Continuous Electron Beam Accelerator Facility for the United States Department of Energy under contract DE-AC05-84ER40150.

ANALYSIS OF SPACE CHARGE CALCULATION IN PARMELA AND ITS APPLICATION TO THE CEBAF FEL INJECTOR DESIGN*

H. Liu

Continuous Electron Beam Accelerator Facility
12000 Jefferson Avenue, Newport News, VA 23606

ABSTRACT

The space charge calculation in PARMELA is analyzed in detail. Two different methods, the 2-D mesh method and the 3-D point-by-point method, are compared based on a cylinder model. Mesh dividing and choice of screening factor for alleviating the numerical noise are discussed and clarified. The analysis is applied to the CEBAF FEL injector design.

INTRODUCTION

Space charge is one of the most intractable issues in designing high intensity charged particle injectors and accelerators. In this respect, it has turned out that PARMELA is suitable for handling an electron bunch of several nC in several ps[1], given that space charge has been calculated properly and all the missing physics have been included.

It seems that the details of the methods for calculating space charge forces in the code are interesting to many users. In this paper, two different methods, the 2-D mesh method and the 3-D point-by-point method[2] are analyzed in detail, and compared based on a cylinder model. Several issues like mesh dividing, choice of screening factor for alleviating the numerical noise, etc. are discussed and clarified. The analysis is applied to the CEBAF FEL injector design.

CYLINDER MODEL

Fig. 1 shows a uniformly charged cylinder in a long metal tube. The cylinder has a radius r_0, a length L, and a charge Q; and the tube has a radius a. The normalized field components e_r and e_z at a point (r, z) inside the cylinder are[3]

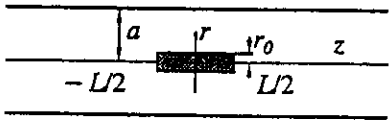

Fig. 1 Cylinder bunch model

$$e_r(u,v) = \frac{2}{\pi}\int_0^\infty S(\alpha\xi)\cos(2\alpha\xi v) I_1(u\xi)[K_1(\xi) + I_1(\xi)K_a]d\xi, \qquad (1)$$

$$e_z(u,v) = \frac{2}{\pi}\int_0^\infty S(\alpha\xi)\sin(2\alpha\xi v)\{1 - \xi I_0(u\xi)[K_1(\xi) + I_1(\xi)K_a]\}\xi^{-1}d\xi, \qquad (2)$$

where $u = r/r_0$ and $v = z/L$, $\alpha = L/2r_0$ the aspect ratio, $K_a = K_0(ka)/I_0(ka)$ the image charge contribution with $k = \xi/r_0$, $S(x) = \sin(x)/x$ the sampling function, and I_n and K_n the nth-order modified Bessel functions. The electric field strength

*Supported by D.O.E. contract #DE-AC05-84ER40150

$E_0 = \sigma_s/2\epsilon_0$ is used for normalization, where ϵ_0 is the vacuum dielectric constant, and $\sigma_s = Q/\pi r_0^2$ the surface charge density. The integral form instead of the series expansion is chosen for its fast convergence.

2-D MESH METHOD

The 2-D mesh method is virtually of a PIC (Particle-In-Cell) scheme. It assumes cylindrical symmetry and the bunch is embedded in an *r-z* mesh in the rest frame. The mesh is specified by *Rmesh Zmesh Nr Nz* and *Frm*, where *Rmesh* and *Zmesh* represent the maximum radial and longitudinal dimensions of the mesh, *Nr* and *Nz* the numbers of radial and longitudinal intervals and *Frm* the factor for enlarging the longitudinal dimension as the bunch is accelerated.

The mesh is designated by two 1-D arrays: *Rm* and *Zm*. Then, as shown in Fig. 2, through integrating over a *finite-size* charged ring corresponding to a bin of the mesh, a background table is established, containing

$$E_n^{(1)}(r_k, z_l) = \sum_{i=1}^{n_2}\sum_{j=1}^{n_1} \frac{R_{mi}}{\bar{R}_m}\lambda_{mi}^{(n2)}\lambda_{mj}^{(n1)}E_{kl}^{(0)}(r_k, z_l; r_{mi}, z_{mj}), \quad \begin{matrix}(k=1,\ldots,Nr+1)\\(l=1,\ldots,Nz)\end{matrix} \qquad (3)$$

where $E_n^{(1)}$ is E_r or E_z at the node (r_k, z_l), $n=(m-1)(Nr+1)Nz+(l-1)(Nr+1)+k$ the sequence number of the field data, n_1 and n_2 the radial and longitudinal numbers of *zero-size* rings in the bin used for integration over $\Delta S = \Delta R \Delta Z$, $\lambda_{mi}^{(n2)}$ and $\lambda_{mj}^{(n1)}$ the 2-D Gaussian integral coefficients, r_{mi} and z_{mj} the location of the zero-size ring within the mth bin, $E_{kl}^{(0)}$ the space charge fields at the node (r_k, z_l) produced by a ring located at (r_{mi}, z_{mj}) in the bin, R_{mi} and $\bar{R}_m$ the radius of the ring (i, j) and the average radius of the corresponding finite-size ring. For a given bin, this integration is done *(Nr+1)Nz* times for all the nodes in the mesh, and then another bin is picked up and the integration is repeated till the last bin at the first column of the mesh (no more than this is necessary because of the symmetry). Therefore *Nr* layers of meshes are established with each layer representing *(Nr+1)Nz* field data at all nodes. Note that n_1 and n_2 are related to the parameter *Opt* on the space charge card *Scheff*.

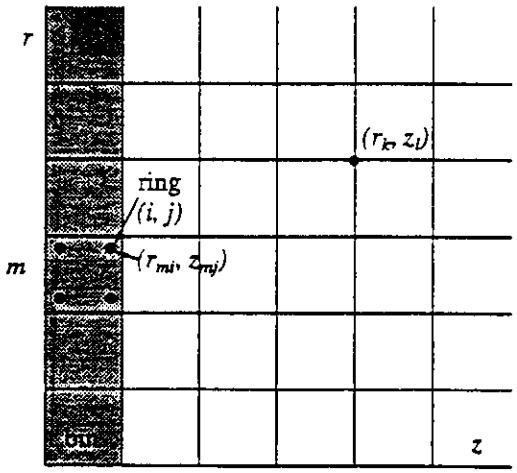

Fig. 2 2-D *r-z* mesh

The second issue is the charge assignment. By shifting a half interval relative to the *Rm-Zm* mesh, another mesh designated by *Rs* and *Zs* has been formed in advance for the use of charge assignment. See Fig. 3, where solid lines correspond to *Rm-Zm* arrays, and dotted lines *Rs-Zs* arrays. The macroparticles are located in the bins in the *Rs-Zs* mesh. Recall that the space charge fields at all nodes have

been calculated previously by assuming a unit and uniform charge distribution in a bin. Now if the charge density in each bin can be found, the space charge fields at all nodes can be calculated by summing up the contributions from all the bins rated by the charge densities assigned to each of them.

Suppose a macroparticle (MP) is located in a bin, as shown in Fig. 3. It occupies an area of $\Delta S = \Delta R \Delta Z$ in the *Rs-Zs* mesh. It can be divided into four parts, *A*, *B*, *C*, and *D*. Then part *A* is assigned to the bin *(i, j)*, *B* to *(i-1, j-1)*, *C* to *(i, j-1)* and *D* to *(i-1, j)*, which constitute the area weighting coefficients for these four bins in the *Rm-Zm* mesh. The assignment is done for all particles. Now the space charge fields at all nodes can be calculated according to

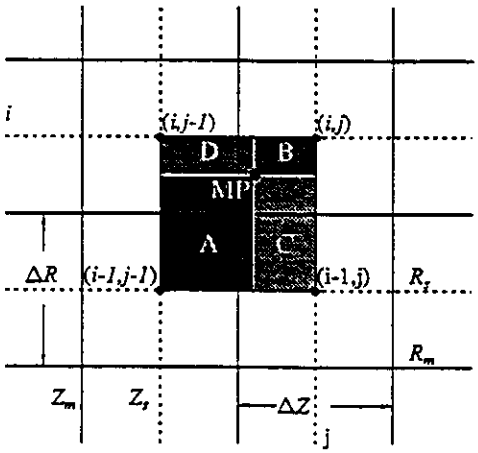

Fig. 3 Charge assignment (MP: MacroParticle)

$$E_n^{(2)}(r_k, z_l) = \sum_{j=1}^{M} A_j E_{nj}^{(1)}(r_k, z_l), \quad \begin{matrix}(k=1,\ldots,Nr+1)\\(l=1,\ldots,Nz)\end{matrix} \tag{4}$$

where $M = Nr \times Nz$ is the total number of bins in the mesh, A_j the charge density weighting coefficient of the jth bin, $E_{nj}^{(1)}$ the contribution to the field at that node from the jth bin, which has been calculated previously according to Eq. (3). The summation goes over all the bins in the *Rm-Zm* mesh.

A space charge field table based on the actual charge distribution has thus been established. Using linear interpolation, the space charge fields at any point possibly occupied by a macroparticle in the mesh can be obtained. Then the fields are transformed to the laboratory frame.

3-D POINT-BY-POINT METHOD

The 3-D point-by-point method is simple. The space charge fields produced by a moving charge Q are calculated in the laboratory frame as follows

$$\mathbf{E} = Q\mathbf{r}/\gamma^2 s^3, \qquad \mathbf{B} = \beta \times \mathbf{E}, \tag{5}$$

where $s = r(1 - \beta^2 \sin^2\theta)^{1/2}$, $\mathbf{r}$ the vector from the source to the observer, $\beta = \mathbf{v}/c$ the normalized velocity, θ the angle between $\mathbf{r}$ and β, and $\gamma = 1/(1-\beta^2)^{1/2}$.

This method does not require any symmetry, which is a great release with respect to the mesh method. However, when a macroparticle is found inside another one, the one applying forces must be screened properly to avoid artificial close-encounter or numerical noise. The screening strongly depends on how the

size of a macroparticle is defined. All the macroparticles have the same rms size which is defined by

$$\sigma^{(MP)}_{x,y,\mathrm{rms}} = \sigma^{(\mathrm{bunch})}_{x,y,\mathrm{rms}}/N_p^{1/3}, \tag{6}$$

where $\sigma^{(\mathrm{bunch})}_{x,y,\mathrm{rms}}$ is the rms size of the total bunch in a specific dimension, and N_P the number of simulated macroparticles. The half width of a macroparticle, e.g., in the x dimension, is correlated with its rms size in the form

$$L^{(MP)}_x = f\sigma^{(MP)}_{x\mathrm{rms}}, \tag{7}$$

where f is the screening factor. A close-encounter is defined by $\Delta x < L^{(MP)}_x$, $\Delta y < L^{(MP)}_y$ and $\Delta z < L^{(MP)}_z$, where Δx, Δy and Δz represent the relative distances between two particles in the x, y and z dimensions. When a close-encounter happens, the macroparticle charge is reduced according to

$$Q^* = Q\frac{\Delta x\Delta y\Delta z}{f^3\sigma_{x\mathrm{rms}}\sigma_{y\mathrm{rms}}\sigma_{z\mathrm{rms}}} < Q. \tag{8}$$

Table 1 Screening Factor

Profile	Screening factor
point	0
ring	1
disk	$\sqrt{2}$
square	$\sqrt{3}$
Gaussian	2
parabolic	$\sqrt{5}$

We found that the screening factor may vary from 0 to $\sqrt{5}$, depending on the density distribution assumed for a macroparticle. See Table 1. In McDonald's version of the code[2], a uniform density profile is assumed. Therefore a screening factor of $\sqrt{3}$ we found here explains the empirical screening factor of 1.75 in Ref. 2.

COMPARISON

The space charge field profiles calculated using PARMELA have been compared with the exact ones from Eqs. (1) and (2) for three different aspect ratios of $\alpha = 10$, 1 and 0.1. In all cases, the bunch has a charge of 6.681 nC, and remains 1 cm in diameter. The bunch length is changed from 10 cm to 1 cm, and in the last case, to 1 mm, to be representative and complete. 10^4 macroparticles are generated uniformly and randomly in the x-y plane but deterministically in the z-dimension. See Fig. 4.

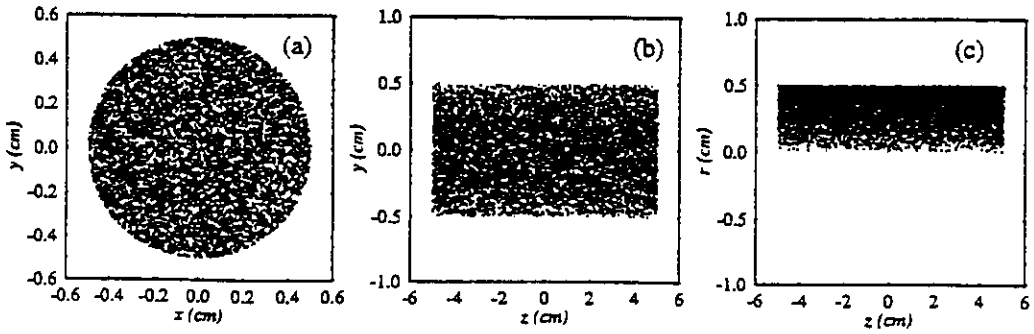

Fig. 4 Bunch model (α=10, Q=6.681 nC, N_p=10^4, (b) & (c) not to scale)

The radial and axial field profiles for $\alpha = 10$ are shown in Fig. 5. They are

obtained by sending a test particle through a specified trace and recording its field response. The abscissas are normalized so that $u = 1$ represents the radial boundary, and $v=\pm 0.5$ the two end planes of the cylinder. The solid smooth curves represent the exact field profiles. The radial field profiles both at the central plane ($v = 0$, solid triangles) and at the end planes ($v = \pm 0.5$, solid and open squares) are demonstrated from (a) to (c). The on-axis axial field profiles (u=0, dots) are indicated from (e) - (f).

From Fig. 5, several interesting points are revealed: (1) the fields are noisier at the central part than at the edges of the bunch; (2) with the screening factor increased from $\sqrt{3}$ to 10 (which is a huge step), the noise can be substantially reduced, but in the meanwhile the particles are over-screened at the edges; (3) the mesh method gives a perfect agreement except at the central part of the bunch with mesh dividing of 40×50.

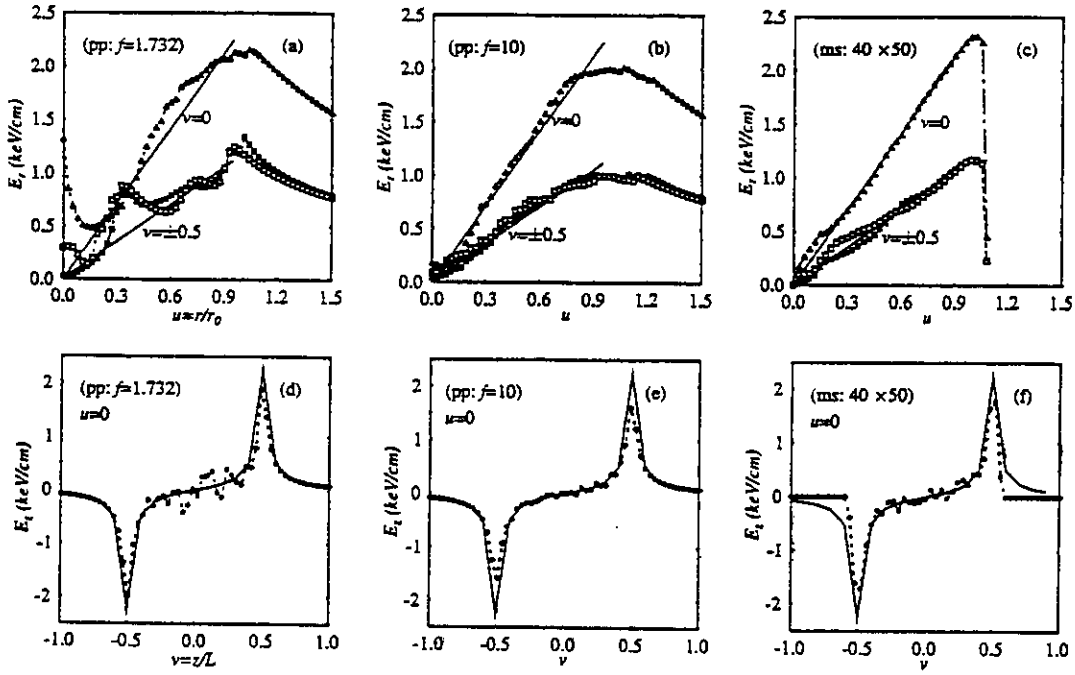

Fig. 5 Comparison between two different methods of space charge calculations in PARMELA. The space charge bunch model is shown in Fig. 4. The aspect ratio α= 10. Abbreviations in the figure: pp - point-by-point method; ms - mesh method; f - screening factor. (a) - (c): radial field profiles at the central plane of the bunch (v=0) and at the end planes of the bunch (v=±0.5). (e) - (f): on axis (u=0) axial space charge field profiles. Solid smooth curves represent the exact field profiles from Eqs. (1) and (2) with image charge omitted. Solid triangles: v=0; solid squares: v=-0.5; open squares: v=0.5.

The results for α=1 are shown in Fig. 6. It is seen that the point-by-point method agrees completely with the exact field expressions out of the bunch ($v=\pm 1$). The agreement for the axial field profile is excellent with a screening factor of $\sqrt{3}$, as shown in (d). It is clear that a smaller screening factor under-screens at the central part but seems precise for the edges, whereas a larger screening fac-

tor over-screens at the edges but seems precise for the central part. We emphasize that it is the edge part of a bunch that needs to be treated more accurately, for that is the region where various nonlinear effects are acting.

The last case is for a very short bunch of 1 mm corresponding to $\alpha = 0.1$. It was claimed that the mesh method seems less suitable for very short bunches[2]

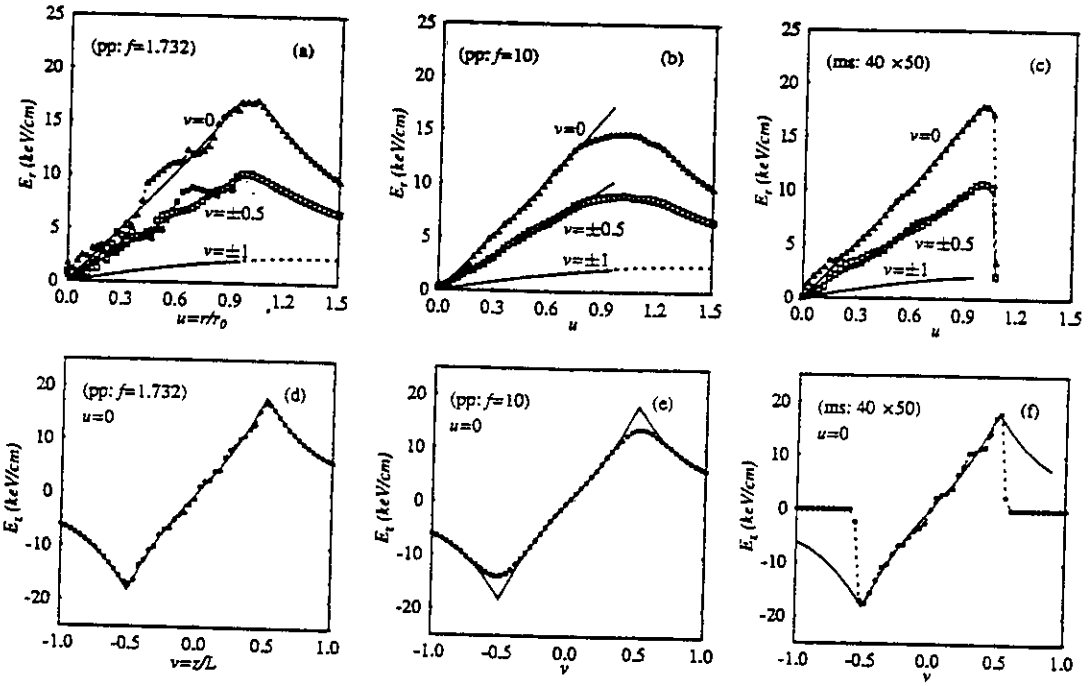

Fig. 6 Same as Fig. 5 except that: (1) the aspect ratio α= 1.0; (2) the radial field profiles out of the bunch (v=±1) are added. Solid smooth curves represent the exact field profiles from Eqs. (1) and (2) with image charge omitted.

and therefore the point-by-point method was developed. Usually, one believes that the aspect ratio is the watershed between the two methods. It was also claimed that the point-by-point method fails because of the artificially large collisions that occur[4]. However, we found that both methods remain accurate for a highly charged short bunch. See Fig. 7.

IMAGE CHARGE

In the mesh method, the image charge is treated based on the ring-model as well. It could be easily proved that[3] a charged ring inside a pipe induces a continuous charge density distribution along the pipe wall as

$$\sigma_z(Z) = \frac{1}{\pi}\int_0^\infty \frac{I_0(k\rho)}{I_0(ka)}\cos(k\Delta Z)dk, \tag{9}$$

where $\Delta Z = Z - Z'$, Z' is the location of the ring, I_0 the *zero*th-order modified Bessel function, ρ the radius of the ring, and a the radius of the pipe. This density distribution is divided into a series of rings along the inside wall of the pipe,

applying forces on other charges. This treatment holds as long as a cylindrical symmetry exists for the bunch.

The point-by-point method deals with the image charge simply as it is. When a particle is emitted from a cathode, it has an image on the other side of the cathode plane; when a particle is inside a metal pipe, it has an image outside the pipe. The image of a macroparticle applies forces on others as if it was a member at a distance from the ensemble.

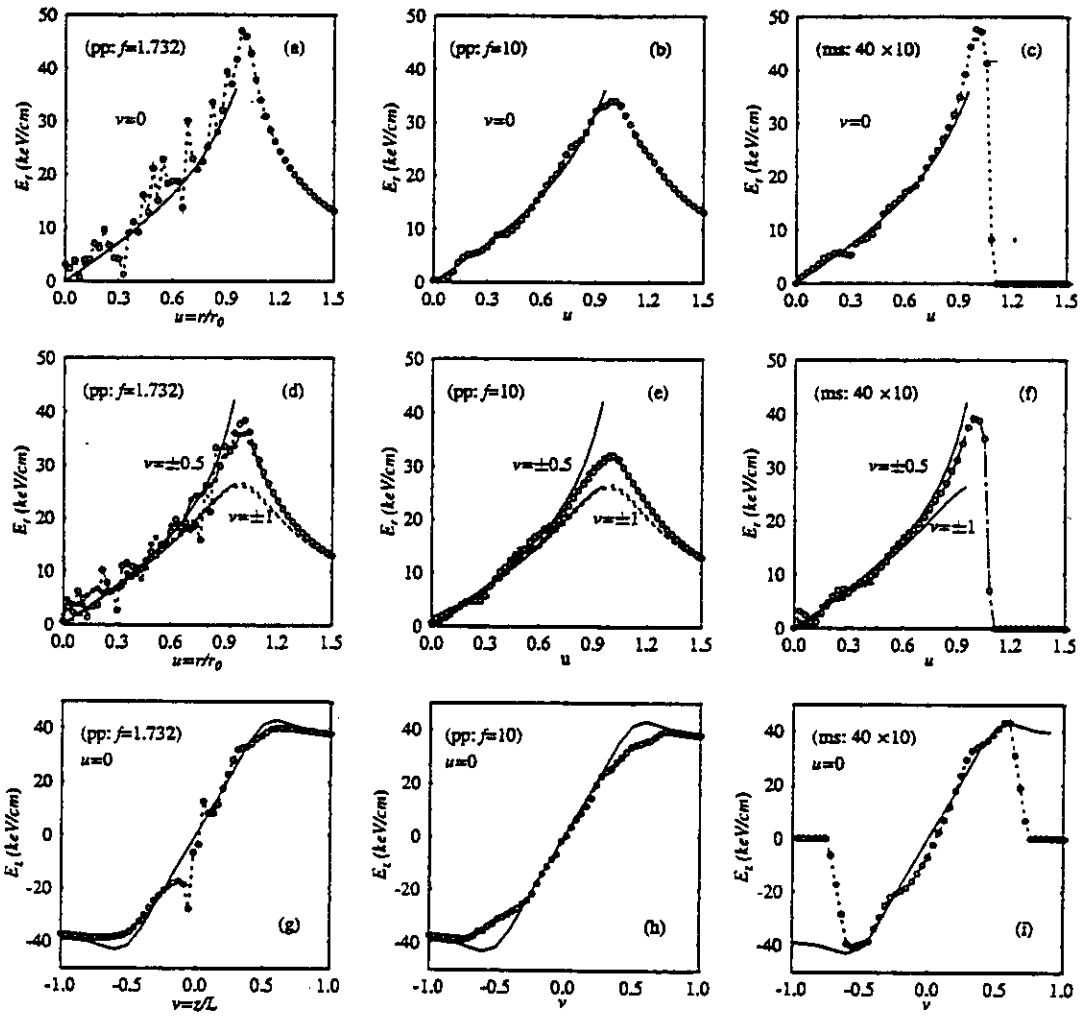

Fig. 7 Same as Fig. 5 except that: (1) the aspect ratio α= 0.1; (2) the radial field profiles out of the bunch ($v=\pm1$) are added; (3) mesh dividing changed from 40×50 to 40×10. Solid smooth curves represent the exact field profiles from Eqs. (1) and (2) with image charge omitted.

APPLICATION

PARMELA has been used for a free-electron laser (FEL) injector design at CEBAF for which the space charge effect is important. CEBAF proposes to build an IR FEL and a UV FEL utilizing the superconducting accelerator technology that has been developed at CEBAF[5,6]. The FEL injector consists of a photo-

cathode DC gun, a prebuncher, a cryounit containing two standard CEBAF SRF cavities, and a phase-compressor chicane. The DC laser gun will be operated at $\sim$ 500 kV and generate a cw train of bunches having a charge of 120 pC and a length of $\sim$ 100 ps from a $\sim$3-mm-diameter photocathode[7].

Based on the previous calculation[8], extensive integrated numerical simulations have been conducted with the point-by-point method for space charge treatment from the cathode all the way down to the exit of the chicane. The injector performance has been fully investigated based on an optimized baseline design for its robustness, sensitivity, and operational flexibilities. The effects of space charge on the phase spread, energy spread and emittance of the electron bunches have been closely examined. It is shown that the design will perform beyond the specifications. The results will be presented elsewhere[9].

SUMMARY

It has been revealed that both methods remain suitable for very short bunches as long as a proper screening factor is introduced for the point-by-point method and a proper mesh is divided for the mesh method. We suggest to set 40×50 as the limit for mesh dividing. The reason is that the space charge is always overestimated at the central part, which could be alleviated if a larger radial nodal number is allowed.

It is emphasized that the number of macroparticles per cell must be significantly larger than unity for both methods. For the mesh method, this means $N_p/N_rN_z >> 1$. For the point-by-point method, it means that the condition $N_p >> f^3$ must be satisfied. We suggest to choose $f \in \{\sqrt{3}, 0.5N_p^{1/3}\}$.

Finally, it is worthwhile to mention that the method introduced in Ref. 4 might be most promising for accurate but less time-consuming 3-D space charge calculations. It would be helpful if a comparison could be made between that method and the point-by-point method on the basis of an appropriate screening factor using a 3-D bunch model.

ACKNOWLEDGEMENT

I wish to thank R. Li for helpful discussions.

REFERENCES

1. B. E. Carlsten *et al.*, IEEE J. of QE, 27, 2580 (1991).
2. K. T. McDonald, IEEE Trans. ED, 35, 2052 (1988).
3. H. Liu, 1989, unpublished.
4. R. W. Garnet and T. P. Wangler, IEEE PAC, 1, 330(1991).
5. J. Bisognano *et al.*, NIM A318, 216(1992).
6. G. R. Neil *et al.*, *ibid.*, p. 212.
7. C. K. Sinclair, *ibid.*, p. 410.
8. P. Liger *et al.*, *ibid.*, p. 290.
9. H. Liu, this conference.